

**Summary.** The mechanisms for spin relaxation in semiconductors are reviewed, and the mechanism prevalent in p-doped semiconductors, namely spin relaxation due to the electron-hole exchange interaction, or Bir-Aronov-Pikus mechanism, is presented in some depth. It is shown that the solution of Boltzmann type kinetic equations allows one to obtain quantitative results for spin relaxation in semiconductors that go beyond the original Bir-Aronov-Pikus relaxation-rate approximation. Experimental results using surface sensitive two-photon photoemission techniques show that the relaxation time of the electron spin polarization in p-doped GaAs at a semiconductor/metal surface is several times longer than the corresponding bulk spin relaxation times. A theoretical explanation of these results in terms of the reduced density of holes in the band-bending region at the surface is presented.



---

# Spin- and Energy Relaxation of Hot Electrons at GaAs Surfaces

T. Ohms, K. Hiebbner, H. C. Schneider, and M. Aeschlimann

Department of Physics  
Kaiserslautern University of Technology  
67663 Kaiserslautern  
Germany

## 1 Introduction

Semiconductor technology has relied on the manipulation of electronic charges since the invention of the transistor. The spin degree of freedom of the carriers has been mostly ignored in traditional electronics. In the last few years there has been a push towards the control of the spin dynamics of charged carriers *independently* of their charge. The exploitation of the spin degree of freedom in electronic [1] and opto-electronic devices [2] and the basic physics associated with the control of spins have been dubbed “spintronics.”

Outside of semiconductor electronics, the control of spins has gained tremendous importance in basic and applied physics in connection with magnetic recording techniques. [3] Metallic materials, which are routinely used for these purposes, have some disadvantages compared to semiconductors. For instance, their carrier densities are not freely controllable and they do not possess bandgaps, which makes their use in opto-electronic devices difficult. It would therefore be advantageous to combine some features of magnetic materials with the versatility of semiconductors. However, the decay of the spin polarization in semiconductors limits all information processing and storage capabilities in semiconductors, which is a big difference from conventional electronics that is based on the conserved electronic charge. Spin relaxation and methods to control spin relaxation thus constitute central problems of spintronics. A promising result on the physical limit of spin manipulation by relaxation phenomena is the measurement of a spin lifetime of about 1 nanosecond in n-doped GaAs at low temperatures [4], but the reason for this remarkable result remains an area of active research.

One important requirement for spin-electronic devices, such as the spin transistor, is the efficient injection of spin-polarized carriers into semiconductors. The straightforward implementation by using ferromagnetic metal contacts has proved to be difficult mainly due to the different conductivities of ferromagnetic metals and semiconductors [5], but tunnel injection into non-

magnetic semiconductors was realized by using incoherent electrical tunneling into the target semiconductor from ferromagnetic metals [6]: In tunneling contacts the injected current is proportional to the density of states of the respective material. Different densities of states for spin-up and spin-down electrons in the ferromagnet therefore give rise to a spin-polarized tunneling current leading to injected spin polarizations of up to 30%. An alternative to the spin injection via interfaces between ferromagnetic metals and semiconductors is the use of magnetic semiconductors instead of ferromagnets. For instance, doping II-VI and III-V semiconductors with Mn can lead to paramagnetic, e.g., BeMnZnSe, and even ferromagnetic compounds such as GaMnAs [7]. Aside from the intrinsic importance of these structures, they can be used for spin injection into non-magnetic semiconductors [3, 8]. However, these techniques suffer from characteristic drawbacks. For instance, paramagnetic semiconductors based on II-VI compounds, require high magnetic fields. The ferromagnetic GaMnAs, on the other hand, has a relatively low Curie temperature of 150 K and works with spin aligned holes, for which momentum-space scattering in bulk (and quantum-well) semiconductors severely limits the lifetimes. Since these problems with electrical spin injection persist, optical techniques are important not only for probing the spin alignment of the carrier system, but also for the creation of a well-controlled spin alignment at arbitrary temperatures. The experimental techniques described in the following rely on the creation of spin-polarized electrons by optical fields and the emission of carriers from the material using laser pulses, and have the advantage that the spin-polarization can be obtained directly from the carriers, which are freed from the material.

In this contribution, we briefly review some of the mechanisms that lead to the relaxation of spin polarization in semiconductors. We then focus on p-doped GaAs and its prevalent spin-relaxation mechanism, the electron-hole exchange interaction, to show that the relaxation of the spin polarization is determined by the full dynamics of the electronic distribution functions and cannot be described using a simple relaxation rate. Instead, we present theoretical results for the spin-polarization dynamics in p-doped semiconductors using a Boltzmann equation approach. In a second part of this contribution we show how the experimental technique of two-photon photoemission (2PPE) can be used to extract information about spin dynamics at semiconductor surfaces and how it can be applied to semiconductor-metal interfaces like Schottky contacts. Experimental results are presented and theoretically explained.

## 2 Review of Spin-Flip Processes in GaAs

In this section we first give an overview of the electron and hole states accessible by optical excitation of GaAs, and the possibility to create spin-polarized electrons by optical excitation. We then describe the origin of the three most

important processes that lead to spin relaxation. Since they are all connected to the bandstructure of semiconductors, we first discuss some generalities on the semiconductor bandstructure, and how it can be approximately calculated close to center of the Brillouin zone.

## 2.1 Optical Orientation of Photo-Excited Carriers

Optical orientation refers to the creation of a non-equilibrium spin alignment, or preferential spin orientation, by excitation with polarized electromagnetic fields. As mentioned above, in semiconductors this is the most important and versatile process to create spin alignment, or as it is commonly called, spin polarization. In the following, we investigate the microscopic *spin polarization*

$$P = \frac{n_{\uparrow} - n_{\downarrow}}{n_{\uparrow} + n_{\downarrow}} \quad (1)$$

defined in terms of the microscopic, time and momentum (or kinetic energy) dependent carrier densities in the spin-up and spin-down electron bands. The dynamics of the microscopic spin polarization  $P$  determines the relaxation of the macroscopic spin polarization, which is often described by a phenomenological  $T_1$  time. We therefore refer to the *decay of the electron spin-polarization simply as spin relaxation*. The experimental and theoretical results on spin relaxation presented in the following are obtained without external magnetic fields, and should therefore not be confused with the dephasing of *coherent* spin dynamics under the influence of magnetic fields [9, 10], whose macroscopic counterpart is often described by a  $T_2$  time, see also Sec. 3.1. Spin-polarized carriers can be detected in experiments and exploited in electro-optical devices due to the polarization of the emitted light when spin-polarized electrons and holes recombine and emit photons. The bandstructure of GaAs near the fundamental band edge [11] that will be the basis of the following discussion consists of:

- electrons with total spin  $S = \frac{1}{2}$  and spin projection quantum number  $s = +\frac{1}{2} \equiv \uparrow$  and  $s = -\frac{1}{2} \equiv \downarrow$ ,
- heavy holes with total angular momentum  $J = \frac{3}{2}$  and projection quantum number  $j = \pm\frac{3}{2}$ ,
- light holes with total angular momentum  $J = \frac{3}{2}$  and projection quantum number  $j = \pm\frac{1}{2}$ ,
- holes in the “split-off” band with total angular momentum  $J = \frac{1}{2}$  and projection quantum number  $j = \pm\frac{1}{2}$ ,

as shown schematically in Fig. 1. More specifically, one has for the spherically symmetric conduction-band wavefunctions at  $k = 0$  in real space representation

$$\langle \mathbf{x}, \sigma | S, s \rangle = u_c(r) \chi_s(\sigma), \quad \sigma = \uparrow, \downarrow \quad (2)$$

where  $r = |\mathbf{x}|$  is the modulus of  $\mathbf{x}$ . The light and heavy hole valence band wavefunctions at  $k = 0$  are given by

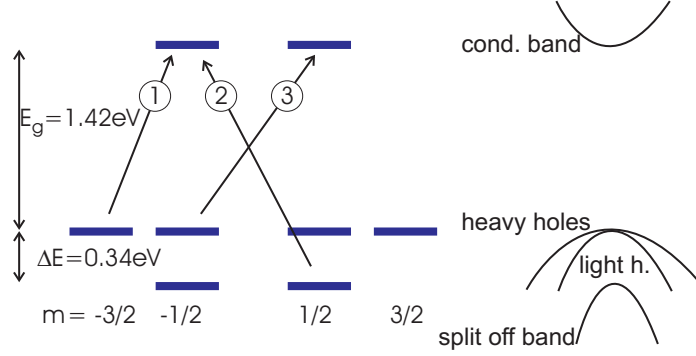


**Fig. 1.** Transitions between electron and hole states induced by circularly polarized light in GaAs at the zone center (left) and schematic bandstructure (right). The angular momentum projection quantum numbers  $m$  shown in the figure apply to all bands above the respective  $ms$ . The relative strengths of the transitions are indicated. For excitation photon energies of less than 1.76 eV, only heavy and light-hole transitions can be driven.

$$\langle \mathbf{x}, \sigma | J = \frac{3}{2}, j = \frac{3}{2} \rangle = Y_{+1}^1(\hat{\mathbf{x}}) \chi_{\uparrow}(\sigma) u_v(r) , \quad (3)$$

$$\langle \mathbf{x}, \sigma | J = \frac{3}{2}, j = \frac{1}{2} \rangle = \frac{1}{\sqrt{3}} \left[ \sqrt{2} Y_0^1(\hat{\mathbf{x}}) \chi_{\uparrow}(\sigma) + Y_{+1}^1(\hat{\mathbf{x}}) \chi_{\downarrow}(\sigma) \right] u_v(r) , \quad (4)$$

$$\langle \mathbf{x}, \sigma | J = \frac{3}{2}, j = -\frac{1}{2} \rangle = \frac{1}{\sqrt{3}} \left[ \sqrt{2} Y_0^1(\hat{\mathbf{x}}) \chi_{\downarrow}(\sigma) + Y_{-1}^1(\hat{\mathbf{x}}) \chi_{\uparrow}(\sigma) \right] u_v(r) , \quad (5)$$

$$\langle \mathbf{x}, \sigma | J = \frac{3}{2}, j = -\frac{3}{2} \rangle = Y_{-1}^1(\hat{\mathbf{x}}) \chi_{\downarrow}(\sigma) u_v(r) , \quad (6)$$

and for the split-off hole wave functions one has

$$\langle \mathbf{x}, \sigma | J = \frac{1}{2}, j = \frac{1}{2} \rangle = \frac{1}{\sqrt{3}} \left[ \sqrt{2} Y_1^1(\hat{\mathbf{x}}) \chi_{\downarrow}(\sigma) - Y_0^1(\hat{\mathbf{x}}) \chi_{\uparrow}(\sigma) \right] u_v(r) , \quad (7)$$

$$\langle \mathbf{x}, \sigma | J = \frac{1}{2}, j = -\frac{1}{2} \rangle = \frac{1}{\sqrt{3}} \left[ Y_0^1(\hat{\mathbf{x}}) \chi_{\downarrow}(\sigma) - \sqrt{2} Y_{-1}^1(\hat{\mathbf{x}}) \chi_{\uparrow}(\sigma) \right] u_v(r) . \quad (8)$$

Here, the  $Y_m^l$  are the spherical harmonics that depend on the direction  $\hat{\mathbf{x}}$  of the vector  $\mathbf{x}$ ,  $\chi_s(\sigma) = \delta_{\sigma,s}$  are spinors, and  $u_c(r)$ ,  $u_v(r)$  contain the radial dependences, which can be obtained from a band-structure calculation. From (2) and (3)–(8) the vectorial dipole matrix elements  $\mathbf{d} = e\mathbf{x}$  for electron-hole transitions can be computed. For instance, choosing the angular momentum quantization axis  $\hat{z}$  perpendicular to the crystal surface and assuming excitation with polarized light propagating in  $z$  direction, one has to evaluate the matrix elements

$$\langle S, s | \hat{\sigma}_{\pm} | J, j \rangle \quad (9)$$

between electron and hole wavefunctions and the polarization vector  $\hat{\sigma}_{\pm} = (\hat{\mathbf{x}} \pm i\hat{\mathbf{y}})/\sqrt{2}$ . Because  $\hat{\sigma}_{\pm} \propto Y_{\pm 1}^1$  this is relatively easy to do. For example, one obtains for the ratio between electron to heavy hole and electron to light-hole transitions

$$\left| \frac{\langle S = \frac{1}{2}, \downarrow | \hat{\sigma}_+ | J = \frac{3}{2}, j = -\frac{3}{2} \rangle}{\langle S = \frac{1}{2}, \downarrow | \hat{\sigma}_+ | J = \frac{3}{2}, j = -\frac{1}{2} \rangle} \right|^2 = 3. \quad (10)$$

These relative magnitudes are indicated in Fig. 1. It is apparent that selective excitation of light and heavy hole transitions will result in an electronic spin polarization of  $P = 0.5$ . In the following, we always assume that an electronic spin polarization is created in this way, and that no split-off holes are populated in the optical excitation process. We will therefore use the abbreviations

$$|j\rangle \equiv |J = \frac{3}{2}, j\rangle, |s\rangle \equiv |S = \frac{1}{2}, s\rangle. \quad (11)$$

Once a spin-polarization is created by optical fields, several mechanisms are known to destroy the spin-polarization. These spin-relaxation mechanisms have been investigated in detail for bulk and, more recently, for quantum-well semiconductors. In the following, we will briefly review the Elliott-Yafet (EY), Dyakonov-Perel (DP), and Bir-Aronov-Pikus (BAP) mechanisms, after some general properties of bandstructure calculations near the fundamental band edge have been discussed.

## 2.2 Bandstructure Properties

The bandstructure of III-V compounds is generally simple at the zone center ( $k = 0$ ). For GaAs, the zone-center wavefunctions of the bands at the fundamental bandgap are given by (2)–(6). For finite  $k$  the energy eigenstates and dipole matrix elements for the bands participating in optical transitions can be determined by perturbation theory starting from the  $k = 0$  states. This is usually done by dividing the bands into those energetically close to the transitions of interest and remote bands. In the case of the interaction with optical fields, the important bands are the heavy hole, light hole, and electron states. Following [12, 13, 14], our starting point is the general form of single-particle carrier states in a periodic potential

$$\psi_{n,\mathbf{k}}(\mathbf{x}, \sigma) = \frac{1}{\sqrt{L^3}} e^{i\mathbf{k} \cdot \mathbf{x}} u_{n,\mathbf{k}}(\mathbf{x}, \sigma) \quad (12)$$

with the crystal volume  $L^3$  and the lattice periodic Bloch function  $u_{n,\mathbf{k}} = |n, \mathbf{k}\rangle$ . The indices  $n$  run over all bands in the semiconductor. A bandstructure calculation in general attempts an approximate solution of

$$H_{\text{carrier}} \psi_{n,\mathbf{k}} = \left[ \frac{1}{2m_0} p^2 + V_{\text{lattice}} + H_{SO} \right] \psi_{n,\mathbf{k}} = \epsilon_{n,\mathbf{k}} \psi_{n,\mathbf{k}} \quad (13)$$

where  $H_{\text{SO}} \propto \mathbf{L} \cdot \mathbf{S}$  is the spin-orbit interaction,  $\mathbf{p} = -i\hbar\nabla$  the linear momentum operator and  $V_{\text{lattice}}$  the periodic potential of the crystal lattice. Equations (12) and (13) lead directly to

$$\left[ H_{\text{carrier}} + H_{kp} + \frac{\hbar^2}{2m_0} k^2 \right] |n, \mathbf{k}\rangle = \epsilon_{n, \mathbf{k}} |n, \mathbf{k}\rangle \quad (14)$$

with

$$H_{kp} = \frac{\hbar}{m_0} \mathbf{k} \cdot \mathbf{p} . \quad (15)$$

At  $k = 0$ , the electron and hole states of interest are eigenstates of the total angular momentum operator and given by (2) and (3)–(8). This set of states will be denoted by  $\mathcal{D}$  in the following. Together with the remote bands at  $k = 0$ , the states  $\mathcal{D}$  satisfy

$$H_{\text{carrier}} |n\rangle = \epsilon_n |n\rangle \quad (16)$$

where  $|n\rangle = |n, k = 0\rangle$  and  $\epsilon_n = \epsilon_{n, \mathbf{k}=0}$ . In the vicinity of  $k = 0$  one can now determine the carrier states  $|n, k\rangle$  by including the coupling of the  $\mathcal{D}$  states with the remote bands via (14) as a 2nd-order perturbation term with interaction matrix element

$$\langle n' | H_{kp}(k) | n \rangle = \frac{\hbar}{m_0} \mathbf{k} \cdot \mathbf{p}_{n'n} \quad (17)$$

where

$$\mathbf{p}_{n'n} = \langle n' | \mathbf{p} | n \rangle . \quad (18)$$

Expanding the states at  $\mathbf{k} \neq 0$  in terms of the states at  $\mathbf{k} = 0$

$$|n, \mathbf{k}\rangle = \sum_m c_{n,m}(\mathbf{k}) |n\rangle \quad (19)$$

leads to the Hamiltonian matrix

$$\begin{aligned} \mathcal{H}_{mn}(\mathbf{k}) = & \left( \epsilon_n + \frac{\hbar^2}{2m_0} k^2 \right) \delta_{m,n} \\ & + \frac{1}{2} \frac{\hbar^2}{m_0^2} \sum_{r \neq m, n} \sum_{\alpha, \beta = x, y, z} p_{n,r}^\alpha p_{r,m}^\beta \left[ \frac{1}{\epsilon_m - \epsilon_r} + \frac{1}{\epsilon_n - \epsilon_r} \right] \end{aligned} \quad (20)$$

determining the single-particle energies  $\epsilon_{n, \mathbf{k}}$  and expansion coefficients in (19) via the eigenvalue problem

$$\sum_{m \in \mathcal{D}} \mathcal{H}_{n'm}(\mathbf{k}) c_{m,n}(\mathbf{k}) = \epsilon_{n, \mathbf{k}} c_{n'n}(\mathbf{k}) . \quad (21)$$

In (20),  $p_{n'n}^\alpha$  is the Cartesian  $\alpha$  component of  $\mathbf{p}_{n'n}$  in (18). The approach outlined above is known as  $k \cdot p$  theory, but the Hamiltonian (20) is usually



replaced by an effective Kohn-Luttinger Hamiltonian containing only a few parameters that can be fitted to experimental results instead of the momentum matrix elements with all the remote bands [12, 11, 14]. In the present case, the general band indices  $m, n$  represent the hole quantum numbers  $j$  or the electron quantum numbers  $s$ . By diagonalizing (21) for each  $\mathbf{k}$ , one obtains the band-structure  $\epsilon_n(k)$  and the coefficients  $c_{n'n}(\mathbf{k})$  determining the states  $|n, k\rangle$  via (19). The advantages of this method to obtain the bandstructure close to  $k = 0$ , are that it avoids a full band-structure calculation, and the effective Hamiltonian can be conveniently parametrized in terms of a few parameters.

The procedure outlined in the previous paragraph yields an effective Hamiltonian that describes the energy splitting of the spin-up and spin-down conduction electron bands in certain crystal directions, and therefore directly yields the Dyakonov-Perel process as will be discussed below. However, it is important to note that this procedure for obtaining effective Hamiltonians is not restricted to the original Hamiltonian (14), but can also be generalized for additional interactions important to the dynamics, such as the Coulomb interaction, the interaction with phonons, or with impurities. Depending on the form of the interaction this leads to additional contributions to the effective Hamiltonian  $\mathcal{H}_{nn'}(\mathbf{k})$  of the general form  $\mathcal{H}_{nn'}^{\text{ph}}(k, k')$  for phonon (or impurity) interaction, which describes scattering with carrier states  $(n, k) \rightarrow (n', k')$ . For the Coulomb interaction, the effective Hamiltonian is an effective two-particle interaction of the form  $\mathcal{V}_{n_1 n'_1 n_2 n'_2}(\mathbf{k}_1, \mathbf{k}'_1, \mathbf{k}_2, \mathbf{k}'_2)$ , which describes the transition, or scattering process,  $(n'_1, k'_1)(n'_2, k'_2) \rightarrow (n_1, k_1)(n_2, k_2)$ . As will be shown below, incorporating the Coulomb interaction leads to the exchange interaction between electrons and holes, i.e., the Bir-Aronov-Pikus process, and carrier-phonon scattering leads to the Elliott-Yafet process.

### 2.3 Elliot-Yafet Mechanism

The Elliot-Yafet mechanism is a spin-flip processes due to the coupling between electrons and holes combined with phonon scattering processes, which can be described by the following effective Hamiltonian [15] including terms to 3rd order in the subspace of the interesting electron bands ( $s, s' = \uparrow$  or  $\downarrow$ )

$$\mathcal{H}_{s's}^{\text{ph}}(k', k) = \sum_j \frac{\mathcal{H}_{s'j}(\mathbf{k}) \langle j | H_{e-p}(k', k) | j \rangle \mathcal{H}_{js}(\mathbf{k})}{(\epsilon_j - \epsilon_s)^2} \quad (22)$$

where  $H_{e-p}$  is the Fröhlich Hamiltonian [16] that describes the long-range interaction with phonons. The Hamiltonian matrix (22) includes the effect the coupling due to the nonvanishing matrix elements  $\mathcal{H}_{sj}(\mathbf{k})$ , cf. (20), between electron and hole states. The phonon scattering process changes the hole momentum  $k \rightarrow k'$ , and therefore, in effect, also changes the mixture of electron and hole states described by the overlap  $\mathcal{H}_{sj}(\mathbf{k})$  since the latter depends on

the wave vector  $k$ . The spin-dependent electronic lifetime<sup>1</sup>

$$\frac{1}{2\tau^{\text{EY}}(k)} = \frac{2\pi}{\hbar} \sum_{\mathbf{k}'} |\mathcal{H}_{\uparrow\downarrow}^{\text{ep}}(k', k)|^2 \delta(\epsilon_{\uparrow, k} - \epsilon_{\downarrow, k'}) \quad (23)$$

is calculated from (22) with Fermi's Golden Rule [15]. As will be discussed in more detail in 3.1, spin-dependent lifetimes are usually interpreted as spin relaxation-times [15], i.e., the relaxation time of the spin *polarization*, but this interpretation is only valid for a low density of electrons very close to equilibrium [23]. Approximately evaluating (23) and averaging over  $k$  using a Maxwell distribution for electrons, results in the spin-relaxation rate [15]

$$\frac{1}{\tau^{\text{EY}}} = C \left( \frac{k_B T}{E_g} \right)^2 \eta^2 \left( \frac{1 - \eta/2}{1 - \eta/3} \right) \frac{1}{\tau_p}. \quad (24)$$

Here,  $E_g$  is the bandgap energy,  $\eta = \Delta_{\text{SO}}/(E_g + \Delta_{\text{SO}})$ ,  $\Delta_{\text{SO}}$  the spin-orbit splitting of the holes,  $\tau_p$  the momentum relaxation-time, and  $C$  a constant which equals 2 for the polar interaction with optical phonons [17]. The EY spin relaxation-time is therefore proportional to the momentum relaxation-time.

## 2.4 Dyakonov-Perel Mechanism

The Dyakonov-Perel (DP) mechanism [18] only occurs in crystals without inversion center because there matrix elements of  $\mathcal{H}_{mn}(\mathbf{k})$  linear and cubic in  $k$  are not forbidden by symmetry [15]. Calculating the effective Hamiltonian for the electronic subsystem taking into account the spin-orbit interaction in the hole subsystem, one finds in these crystals that the spin-degeneracy is lifted by the Dresselhaus term, usually written in the form [15, 18]

$$\mathcal{H}_{ss'}(\mathbf{k}) = \frac{\hbar}{2} \boldsymbol{\Omega}(\mathbf{k}) \cdot \boldsymbol{\sigma}_{ss'}. \quad (25)$$

In (25),  $\boldsymbol{\Omega}(\mathbf{k})$  is a *momentum dependent* vector (cubic in  $k$ ), and  $\boldsymbol{\sigma}_{ss'}$  the vector of Pauli matrices. This effective interaction has the same effect as an external magnetic field with Larmor frequency  $\boldsymbol{\Omega}(\mathbf{k})$ , which can be calculated by taking into account the influence of the spin-orbit interaction with the holes perturbatively. Momentum scattering processes with phonons or impurities will therefore change the effective magnetic Larmor frequency  $\boldsymbol{\Omega}(\mathbf{k})$  experienced by an electron by changing its momentum. An electron therefore experiences a fluctuating magnetic field, which contributes to the electron spin relaxation. Dyakonov and Perel first calculated the spin relaxation-time due to this effect in the collision dominated limit, i.e., when the momentum

---

<sup>1</sup> With the factor of 2 included on the LHS of (23),  $\tau^{\text{EY}}$  can be identified with the spin relaxation-time under certain assumptions.

scattering time is *shorter* than the time scale of the electron-spin precession. This situation corresponds to spin relaxation by repeated small precessions, which is similar to the “motional narrowing” in nuclear magnetic resonance. The DP result is [15]

$$\frac{1}{\tau_{\text{DP}}} = \tilde{C} \alpha^2 \frac{(k_B T)^3}{\hbar^2 E_g} \tau_p \quad (26)$$

where  $\tilde{C}$  is a dimensionless factor of order unity depending on the scattering mechanism and  $\alpha$  is a parameter related to the cubic bandstructure term, given approximately by

$$\alpha \simeq \frac{4\eta}{\sqrt{3-\eta}} \frac{m_e}{m_0}, \quad (27)$$

and  $\tau_p$  the momentum relaxation-time. In (27),  $m_e$  is the effective electron mass in the crystal at  $k = 0$  and  $m_0$  is the free electron mass. The spin relaxation-time (26) due to the DP process is inversely proportional to the momentum relaxation-time. Therefore, the resulting spin relaxation-time is *slower* for faster momentum scattering, leading to the counter-intuitive result that a “dirty” material with strong impurity scattering may have a longer spin lifetime.

## 2.5 Bir-Aronov-Pikus Mechanism

The Bir-Aronov-Pikus (BAP) process is based on the exchange interaction between electrons and holes, which can be calculated from an effective Hamiltonian in 3rd order in the interaction with the remote bands [19]. Since we will treat the BAP process in more depth, and it is a two-particle interaction, we write the Hamiltonian in 2nd quantization

$$H_{\text{exc}} = \sum_{k_1, k_2, q} \sum_{j, s, j', s'} \langle j' s' | \mathcal{V}_{\text{exc}}(\mathbf{q}) | s j \rangle c_{j', k_2+q}^\dagger c_{s', k_1-q}^\dagger c_{j, k_1} c_{s, k_2} \quad (28)$$

Here,  $c_s$  ( $c_s^\dagger$ ) and  $c_j$  ( $c_j^\dagger$ ) are electron and hole destruction (creation) operators [notation as in (11)]. The interaction matrix element [20, 15]

$$\langle j' s' | \mathcal{V}_{\text{exc}}(\mathbf{q}) | s j \rangle = \langle j' s' | \mathcal{V}_{\text{SR}}(\mathbf{q}) | s j \rangle + \langle j' s' | \mathcal{V}_{\text{LR}}(\mathbf{q}) | s j \rangle \quad (29)$$

consists of a long-range part

$$\langle j' s' | \mathcal{V}_{\text{LR}}(q) | s j \rangle = \frac{\hbar^2}{m_0^2} \frac{(\mathbf{q} \cdot \mathbf{p}_{j's})(\mathbf{q} \cdot \mathbf{p}_{s'j})}{(\epsilon_s - \epsilon_{j'})^2} \quad (30)$$

and a short-range part

$$\langle j' s' | \mathcal{V}_{\text{SR}}(q) | s j \rangle = \frac{3}{2} \Delta_{\text{exc,SR}} \langle j', s' | \left[ \frac{3}{4} + (\mathbf{J} \cdot \mathbf{S}) \right] | j, s \rangle \quad (31)$$

In (30), the  $\mathbf{p}_{js}$  are the matrix elements of the momentum operator between the states (11) defined in (18). In (31),  $\Delta_{\text{exc,SR}}$  is the excitonic exchange splitting,  $\mathbf{J}$  is the hole total angular momentum operator and  $\mathbf{S}$  is the electron spin operator. For an explicit matrix representation of (30) and (31), see [21, 20, 15]. It should be noted that (28), (30), and (31) are written with the customary definition of two-particle interaction matrix elements [22]. The order of the indices shows that (28) describes an electron-hole exchange interaction process, i.e., an *interband* scattering process.

Using these contributions, BAP derived a  $k$  dependent electron spin lifetime using Fermi's Golden Rule [19, 15]<sup>2</sup>

$$\frac{1}{2\tau_s^{\text{BAP}}(k)} = \frac{2\pi}{\hbar} \sum_{\mathbf{q}, \mathbf{p}} \sum_{j, j'} |\langle j' s' | \mathcal{V}(\mathbf{q}) | s j \rangle|^2 n_{j,p} (1 - n_{j', \mathbf{p}-\mathbf{q}}) \times \delta(\epsilon_{s,k} + \epsilon_{j,p} - \epsilon_{s', \mathbf{k}+\mathbf{q}} - \epsilon_{j', \mathbf{p}-\mathbf{q}}) \quad (32)$$

where  $s' \neq s$  is the flipped spin. As mentioned in Sec. 2.3, lifetimes derived from Fermi's Golden Rule [15] are usually identified with the spin relaxation-time, but this identification breaks down for higher electronic densities or pronounced non-equilibrium situations [23]. For a low density *thermalized* electron distribution, one can thermally average (32) with a Maxwell distribution to obtain [15, 24]

$$\frac{1}{\tau_{\text{BAP}}} = \frac{2a_B^3}{\tau_0} \frac{v_F \epsilon_{s,k}}{v_B \epsilon_F} N_A. \quad (33)$$

Here,  $a_B$  and  $v_B$  are the Bohr radius and velocity of the exciton,  $\epsilon_F$  and  $v_F$  the hole Fermi energy and velocity,  $N_A$  the total concentration of holes, and

$$\frac{1}{\tau_0} = \frac{3\pi}{64} \frac{\Delta_{\text{exc,SR}}^2}{E_B \hbar} \quad (34)$$

where  $E_B$  is the excitonic binding energy and  $\Delta_{\text{exc,SR}}$ , as defined above, is the excitonic exchange splitting.

### 3 Spin-Polarization *Dynamics*

#### 3.1 Theory of Spin-Relaxation Dynamics

Electron-spin dynamics in general can be described by the reduced one-particle density matrix [25, 29]

$$\rho_{s,s'} = \begin{pmatrix} \rho_{\uparrow\uparrow} & \rho_{\uparrow\downarrow} \\ \rho_{\downarrow\uparrow} & \rho_{\downarrow\downarrow} \end{pmatrix} \equiv \begin{pmatrix} n_{\uparrow} & \psi \\ \psi^* & n_{\downarrow} \end{pmatrix} \quad (35)$$

with the real average electronic occupation numbers and the complex spin-coherence  $\psi$  that are driven by a magnetic field. The spin coherence is only

<sup>2</sup> The factor 2 in the following is the same as in (23).

nonzero if the spin-up and spin-down states are no longer eigenstates of the Hamiltonian, i.e., when the electrons are coupled by an external magnetic field or an effective internal magnetic field as it is the case for the Dyakonov-Perel mechanism. The dynamics of electrons in a magnetic field therefore follows the equations of motion for the time-dependent electron distributions  $n_\uparrow$ ,  $n_\downarrow$  and the spin coherence  $\psi$  as defined by (35) [25, 10]. In semiconductors, both these quantities are subject to carrier-carrier and carrier-phonon scattering. The microscopic description of the different interaction mechanisms does not, in general, allow the introduction of macroscopic  $T_1$  and  $T_2$  times [24]. If these approximate quantities can be introduced for interacting electrons in semiconductors,  $T_1$  refers to the relaxation of the macroscopic spin polarization toward its equilibrium  $P = 0$  value. For this to happen, the angular momentum has to be transferred out of the electron system to the holes and eventually to the lattice. This has to be kept apart from the decay of the spin coherence which is described by  $T_2$  at the macroscopic level. Thus  $T_2$  is a measure of the dephasing of the electron spin-coherence driven by magnetic fields and usually called “homogeneous broadening” analogous to the case of nuclear magnetic resonance. If there are additional contributions to the dephasing related to “inhomogeneous” broadening due to, e.g., spatial fluctuations of the magnetic field, one sometimes describes the combined effect of the inhomogeneous broadening and the homogeneous broadening on the decay of the macroscopic spin coherence by  $T_2^*$  [24].

In a magnetic field one has two contributions to the time development of the spin polarization  $P$ : one is due to the *incoherent* spin-flip processes related to  $T_1$  and the other due to the coherent change of the electronic distribution functions as long as there is a spin coherence driven by a magnetic field. For the study of the spin polarization relaxation it can therefore be advantageous to consider the case without magnetic fields, as will be done here, because this eliminates the influence of *coherent* magnetic-field induced spin-flips. In the following, we will deal only with the *incoherent* spin-polarization relaxation, i.e., the time development of (1) and its momentum (or energy) dependent generalization

$$P_k = \frac{n_{\uparrow,k} - n_{\downarrow,k}}{n_{\uparrow,k} + n_{\downarrow,k}}. \quad (36)$$

A preliminary understanding of the spin relaxation can be achieved using lifetimes as they result from a Fermi’s Golden Rule treatment as outlined in Sec. 2.5. Consider for definiteness the BAP-process, for which the spin lifetime is described by (32). Since Fermi’s Golden Rule yields lifetimes, this is equivalent to a relaxation-time approximation of the form [23]

$$\left. \frac{\partial}{\partial t} n_s(k) \right|_{\text{BAP}} = -\frac{1}{2\tau_s^{\text{BAP}}(k)} [n_s(k) - f_s(k)] \quad (37)$$

where  $f_s(k)$  is an equilibrium (Fermi-Dirac) distribution, to which the system relaxes. In addition to this relaxation of the electronic distributions, one has

to take into account that the scattered electrons, which flip their spins during the scattering processes, have to be accounted for in the number of carriers in the electronic band with opposite spin. Using this reasoning for a nonzero electronic spin polarization and an *unpolarized* hole system, i.e.,  $n_{j=\frac{3}{2},k} = n_{j=-\frac{3}{2},k}$  and  $n_{j=\frac{1}{2},k} = n_{j=-\frac{1}{2},k}$ , one finds from (32)

$$\tau_{\uparrow}^{\text{BAP}}(k) = \tau_{\downarrow}^{\text{BAP}}(k) , \quad (38)$$

and further obtains

$$\left. \frac{\partial}{\partial t} P_k \right|_{\text{BAP}} = -\frac{P_k}{\tau_s^{\text{BAP}}(k)} . \quad (39)$$

This result reflects the physical situation that the spin polarization decays, if the different populations relax towards equilibrium according to (37), but the scattered electrons show up in the band with opposite spin with the same momentum after the scattering process. The information about the energy and momentum dependence of spin-flip scattering is therefore lost in this approximation. As will be shown below, the treatment of electron dynamics as scattering processes without the relaxation-time approximation leads to a more general description of spin polarization dynamics due to the exchange interaction. It is interesting to note that the field of spin relaxation has been dominated by rate-equation approximations for decades [26], but efforts have been made recently to go beyond this approximation for the description of spin-dependent scattering phenomena [27, 28, 29, 30].

Since the experimental results discussed below are for heavily p-doped GaAs, the following the discussion will focus on the spin dynamics due to the electron-hole exchange interaction (28), i.e., the BAP process. To go beyond Fermi's Golden Rule one derives the dynamical equations for the relevant correlation functions in the electronic ensemble, which are the distribution functions for electrons

$$n_{sk}(t) = \langle c_{sk}^{\dagger} c_{sk} \rangle , \quad (40)$$

defined with time-dependent creation and destruction operators in the Heisenberg picture. The symbols  $\langle \dots \rangle$  designate a statistical average over the ensemble of electrons. The dynamics of the carrier distributions  $n_{sk}$  is then determined by the Heisenberg equation of motion

$$\frac{\hbar}{i} \frac{\partial}{\partial t} \langle c_{sk}^{\dagger} c_{sk} \rangle = \langle [H, c_{sk}^{\dagger} c_{sk}] \rangle . \quad (41)$$

With a two-particle interaction Hamiltonian such as  $H_{\text{exc}}$  in (28), one runs into the well-known hierarchy problem that the equations of motion for the carrier distributions  $n_{sk}$  do not close, i.e., they couple to correlation functions containing two creation and two destruction operators. The hierarchy problem can be approximately solved, e. g., using Green's functions [31, 32] or truncation [33, 34] techniques. Technically, the random-phase approximation (RPA) will be employed in the following. One obtains as the dynamical equation for

the spin-flip scattering due to electron-hole exchange interaction a Boltzmann equation

$$\left. \frac{\partial}{\partial t} n_{sk} \right|_{\text{BAP}} = -\Gamma_{sk}^{\text{BAP,out}} n_{sk} + \Gamma_{sk}^{\text{BAP,in}} (1 - n_{sk}) \quad (42)$$

with spin and momentum dependent out-scattering

$$\begin{aligned} \Gamma_{sk}^{\text{BAP,out}} = \frac{2\pi}{\hbar} \sum_{\mathbf{q}, \mathbf{p}} \sum_{j, j'} |\langle j' s' | \mathcal{V}_{\text{exc}}(\mathbf{q}) | s j \rangle|^2 n_{j, \mathbf{p}} (1 - n_{j, \mathbf{p}-\mathbf{q}}) (1 - n_{s', \mathbf{k}+\mathbf{q}}) \\ \times \delta(\epsilon_{s, k} + \epsilon_{j, p} - \epsilon_{s', \mathbf{k}+\mathbf{q}} - \epsilon_{j', \mathbf{p}-\mathbf{q}}) \end{aligned} \quad (43)$$

and in-scattering rates

$$\begin{aligned} \Gamma_{sk}^{\text{BAP,in}} = \frac{2\pi}{\hbar} \sum_{\mathbf{q}, \mathbf{p}} \sum_{j, j'} |\langle j' s' | \mathcal{V}_{\text{exc}}(\mathbf{q}) | s j \rangle|^2 (1 - n_{j, \mathbf{p}}) n_{j', \mathbf{p}-\mathbf{q}} n_{s', \mathbf{k}+\mathbf{q}} \\ \times \delta(\epsilon_{s, k} + \epsilon_{j, p} - \epsilon_{s', \mathbf{k}+\mathbf{q}} - \epsilon_{j', \mathbf{p}-\mathbf{q}}) . \end{aligned} \quad (44)$$

Here,  $s' = -s$  is the flipped spin quantum-number, and the interaction matrix element is given by (29). One notices that the out-scattering rate is identical to the lifetime obtained by Fermi's Golden Rule (32) if the electronic occupation of the final state, into which the spin-flipped electron is scattered, is small, i.e., if  $n_{s', \mathbf{k}+\mathbf{q}} \ll 1$ . Also, a term mimicking the effect of the in-scattering term in the Boltzmann equation had to be added to the relaxation-time equation by hand, since Fermi's Golden rule yields only a lifetime, i.e., a decay time for individual electrons due to the spin-flipping exchange interaction.

Formally, a similar Boltzmann equation describes the time development of the hole distribution functions under the action of the electron-hole exchange scattering. As will be shown later experimentally and theoretically, the spin-flip scattering (42) due to the electron-hole exchange interaction takes place on a timescale of several ten picoseconds in moderately to strongly p-doped GaAs. We are here exclusively interested in p-doped GaAs where a large density of holes and a very small density of electrons is present. Thus the hole angular momenta equilibrate due the rapid momentum scattering and spin-orbit interaction much faster than the electronic spins. We will therefore treat the holes only as a bath in the following calculations.

In addition to the electron-hole exchange interaction, carriers interact also via the *direct* Coulomb interaction. This leads to strongly carrier-density dependent scattering times that reach several hundred femtoseconds for high carrier densities. We therefore have to include the effect of the fast direct electron-hole Coulomb scattering, which is spin conserving, in addition to the spin-flip electron-hole exchange scattering since the electronic distribution functions in (42) will evolve under the action of the direct scattering quickly. This is described by the well-known Boltzmann equation for the direct Coulomb scattering in random-phase approximation [35]

$$\begin{aligned}
\left. \frac{\partial}{\partial t} n_{sk} \right|_{\text{Coul}} &= -\frac{2\pi}{\hbar} \sum_{k'qj} |W_q|^2 [n_{sk}(1 - n_{sk+q})n_{jk'+q}(1 - n_{jk'}) \\
&\quad - (1 - n_{sk})n_{sk+q}(1 - n_{jk'+q})n_{jk'}] \\
&\quad \times \delta(\epsilon_{jk+q} + \epsilon_{sk} - \epsilon_{jk'} - \epsilon_{sk+q}) . \quad (45)
\end{aligned}$$

Here,  $W_q = V_q/\varepsilon_q$  is the screened Coulomb interaction in momentum space defined in terms of the bare Coulomb interaction

$$V_q = \frac{e^2}{\varepsilon_0 \varepsilon_{\text{bg}} q^2} \quad (46)$$

with the background dielectric function  $\varepsilon_{\text{bg}}$ . The carrier contribution to the dimensionless dielectric function is calculated in static approximation  $\varepsilon_q = 1/(1 + q^2/\kappa^2)$  where  $\kappa$  is the screening wavevector [35].

Equations (42) and (45) define our model that will be used to calculate the dynamics of electronic distribution functions and thus the spin relaxation. We will neglect electron-electron Coulomb scattering because the electronic densities will be kept so low that this process is much slower than the electron-hole Coulomb scattering. We will also use fixed Fermi-Dirac distributions for the high-density hole distributions because the fast hole-hole Coulomb scattering together with the spin-orbit interaction keeps the hole system in thermal equilibrium and prevents the occurrence of hole spin polarization on timescales important for the electronic spin dynamics.

### 3.2 Numerical Results

In this section results of the numerical solution of (42) and (45) are presented. The numerical solution is accomplished by transforming the sums into integrals and then using a 4th order Runge-Kutta algorithm to calculate the time evolution of the electronic distribution functions. The initial conditions in the following are always taken to be quasi-equilibrium distributions for electrons and holes. After optical excitation of spin polarized carriers in p-doped GaAs the electrons will quickly equilibrate thermally without losing their spin coherence on this timescale, whereas the holes will lose their spin polarization due to spin-orbit interaction and Coulomb scattering so that one can assume quasi-equilibrium conditions with polarized electrons and unpolarized holes.

As a first result of the model we will discuss the interplay between direct Coulomb scattering and exchange scattering. Figure 2 shows the result of a numerical experiment, in which the case with Coulomb scattering is compared to the one where Coulomb scattering is “switched off.” For the case of a polarized low electron density at 300 K in the presence of an high density of unpolarized holes at 600 K, one finds that the direct Coulomb interaction has a significant influence on the dynamics of the electron spin polarization over several tens of picoseconds, even though the characteristic timescale of direct Coulomb scattering is on the order of a few hundred femtoseconds. Thus the



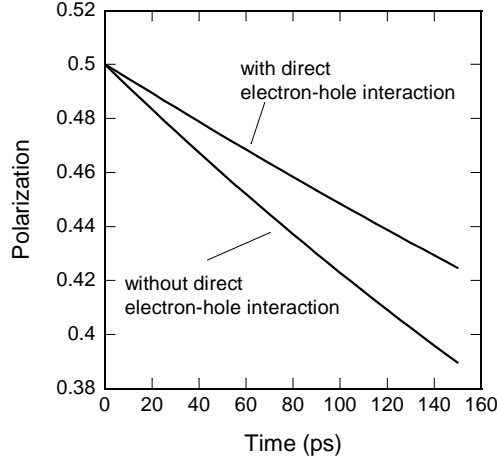


**Fig. 2.** Computed relaxation of electron spin polarization  $P(t)$  for electron-hole exchange interaction with direct Coulomb interaction (top curve) and exchange interaction without Coulomb interaction (bottom curve). At  $t = 0$ , carrier temperatures, densities and spin polarizations are 300K,  $10^{18} \text{ cm}^{-3}$  and 0% for holes, and 600 K,  $10^{15} \text{ cm}^{-3}$  and 50% for electrons, respectively.

direct scattering influences the dynamics of the electron spin polarization, even though it does not give rise to spin flips. The reason for this behavior is that the exchange scattering alone creates non-equilibrium electron distributions over time, whereas the direct scattering continually drives the electronic distributions into equilibrium with the holes. The resulting competition leads to the faster electron spin-polarization decay if both scattering mechanisms are included. It should also be noted that, even though the time-development of the total polarization is plotted here, the time development of the energy-resolved spin polarizations are not much different from the total polarization. In the range of electron and hole temperatures around room temperature, the energy-resolved polarization and the total polarization can be fitted with an exponential decay law, and the time constants are practically equal for all those quantities. In the case of Fig. 2 we find a relaxation time of 950 ps for the electronic polarization.

Figure 3 shows the energy-dependent out-scattering rate (43) for electrons due to the exchange interaction with unpolarized holes, with all the parameters being the same as before. It should be noted that the out-scattering rate is identical to the Fermi's Golden Rule result in the low electron-density limit. This quantity was calculated earlier for  $T = 0 \text{ K}$  [21] as a measure of the spin relaxation time, which was predicted to be strongly energy dependent on the basis of this calculation. However, as mentioned in connection with Fig. 2, no

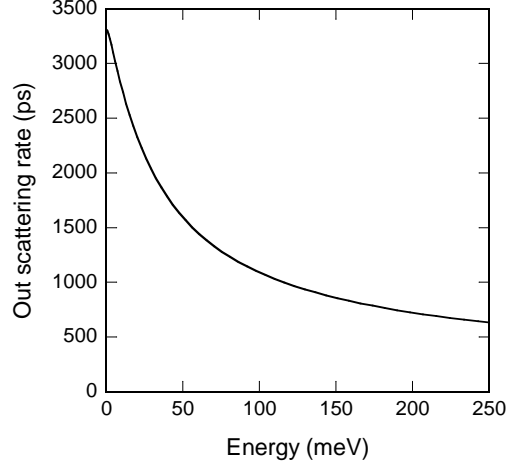


**Fig. 3.** Calculated out-scattering rate (43) vs. electronic energy for the same parameters as in Fig. 2.

energy-dependence of the spin-polarization relaxation is found in our numerical results including the dynamics due to both exchange and direct scattering processes.

Figure 4 shows the computed spin relaxation-time for different hole concentrations. For the range of densities depicted in Fig. 4, the dynamics of electron spins was calculated over 180 ps, and an exponential fit was made to the resulting polarization dynamics. The result is a meaningful measure of the effectiveness of the BAP process for the polarization relaxation that can be compared to experiments. For a high doping concentration of  $N_A = 10^{19} \text{ cm}^{-3}$  we obtain a spin relaxation time of 110 ps, which is in very good agreement with recent measurements of the bulk spin relaxation in identical samples using time-resolved Faraday rotation techniques [36]. In principle, one can therefore use the calculated density dependence of the spin relaxation-time to obtain an estimate of the hole density and thus the doping concentration in a GaAs/metal interface (Schottky barrier), where the band bending near the surface leads to a depletion of holes in the vicinity of the surface. Before we turn to the discussion of the experimental setup and the experimental results, we briefly review the concept of a Schottky contact and the band bending at semiconductor-metal surfaces.

### 3.3 Spin Decay in a Schottky-Barrier

Most metal-semiconductor interfaces act as a diode because the electric current passing through the interface depends exponentially on the forward bias

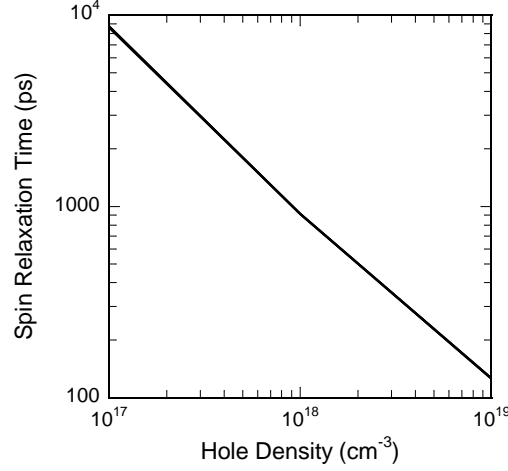


**Fig. 4.** Calculated spin relaxation-time vs. density of holes for hole temperature of 300 K, electron density  $10^{14} \text{ cm}^{-3}$  and temperature 600 K. The initial polarization is again  $P(t=0) = 50\%$ .

since a depletion layer in the semiconductor builds up [37, 38]. These contacts are known as “Schottky contacts,” as opposed to ohmic contacts which have a lower resistance. The concept of a depletion layer and the accompanying band bending is most easily described for a semiconductor vacuum surface before moving on to the actual Schottky contact [37].

Consider a uniformly p-doped semi-infinite slab of semiconductor material, where the majority of carriers are holes, and the doping concentration is  $N_A$ . The introduction of a surface breaks the crystal symmetry and leads to additional carrier states located near the surface, whose energies lie in the semiconductor bandgap and which are occupied predominantly by holes in a p-doped semiconductor. The holes occupying the surface states lead to a positive surface charge  $\sigma$  and must have come from acceptors in a region of width  $w$  beneath the surface, the so-called depletion layer, where there is now a negative space charge  $\varrho = -eN_A$  per unit volume, see Fig. 5. (Here,  $e > 0$  denotes the magnitude of the electronic charge.) Charge neutrality requires

$$\sigma + \varrho w = 0. \quad (47)$$

The positive space charge of the depletion layer now causes an electrostatic potential, which is responsible for the characteristic band bending. This, in turn, reduces the surface charge and compensates it almost completely. To see this, one calculates the electrostatic potential  $\Phi(z)$  away from the surface induced by the space charge of the depletion layer according to Poisson’s law

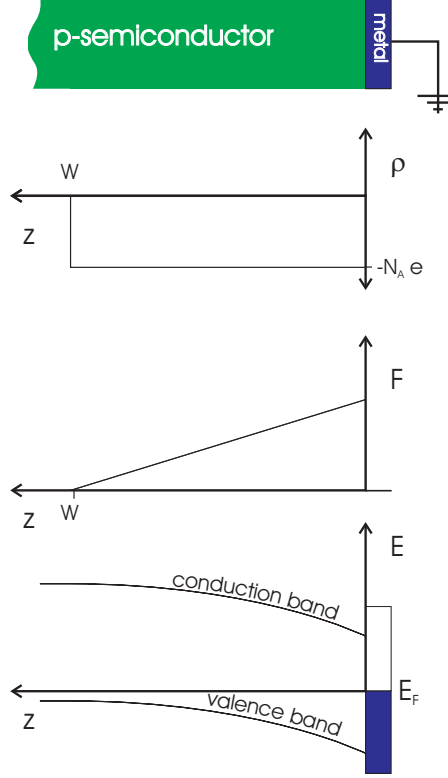


**Fig. 5.** Schottky contact between p-doped semiconductor and metal. The charge distribution  $\rho$  is approximated as a step function, leading to the electric field distribution and band lineup shown below.

$$\frac{d^2}{dz^2}\Phi(z) = -\frac{\rho}{\varepsilon_b\varepsilon_0}, \quad (48)$$

where  $\varepsilon_b$  and  $\varepsilon_0$  are the permittivity of the semiconductor and the vacuum, respectively. In solving the equation for  $\Phi(z)$  we assume that at the end of the depletion layer ( $z = w$ ) we can set the electrostatic potential  $\Phi$  and the field  $\mathcal{F} = -d\Phi/dx$  to zero. We find a simple linear dependence for the electric field

$$\mathcal{F}(z) = -\frac{\rho}{\varepsilon_b\varepsilon_0}(w - z) \quad (49)$$

and for the potential accordingly

$$\Phi(z) = -\frac{\rho}{2\varepsilon_b\varepsilon_0}(w - z)^2. \quad (50)$$

Thus the additional potential energy for an electron with charge  $q = -e$  in the the region  $z < w$  is  $-e\Phi(z)$ , leading to a downward band-bending.

With this background discussion one can turn to the metal-semiconductor Schottky contact [37], and consider again the case of a p-type semiconductor. It is assumed that the metal has a chemical potential, which is denoted by the Fermi energy  $E_F$ , and the semiconductor has a chemical potential  $\mu$ . Before bringing the two materials into contact the respective chemical potentials are different, with the semiconductor chemical potential lying in the bandgap close to the valence band because of the p-doping, and therefore lower than the metal chemical potential. Bringing the two materials together sets up an electric field due to the different chemical potentials which drives electrons into the semiconductor, thereby creating a negative space charge in the semiconductor and a positive surface charge, just as in the example discussed above. When the materials are joined, these two charge distributions balance each other. Also, the common chemical potential is pinned because the surface (or interface) states are only partially filled. The negative space charge in the semiconductor leads to the band bending described above, as shown in Fig. 5.

When carriers are created in the semiconductor away from the surface by optical excitation near the bandgap, this band configuration is the reason that diffusion of optically excited electrons from the bulk towards the surface yields electrons with a high kinetic energy, i.e., “hot” electrons, at the surface [39].

## 4 Experiments

### 4.1 Time and Spin Resolved 2PPE

Carrier spin-relaxation measurements in zero applied field have been reported in [9] by means of time-resolved Faraday rotation experiments. In order to isolate the spin decay occurring only in the band-bending region, a surface sensitive and energy resolving technique is needed. To explore the spin- and charge dynamics in this region we introduce a novel real-time method. We use a pump-probe approach referred to as time-resolved 2-photon-photoemission (TR-2PPE) with the additional option to measure the spin-polarization of the emitted electrons [40]. By varying the time delay between the ultrashort pump and probe laser pulses, the spin-dependent population decay of the intermediate (unoccupied) states can be determined. The high surface sensitivity as well as the energy selectivity of the photoemission technique is appropriate to investigate the spin dynamics in the Schottky barrier. From this perspective, TR-2PPE is complementary to Faraday rotation. In TR-2PPE one simply determines the spin polarization  $P$  defined in (36) of the transient carrier concentration in a certain energy interval. The energy-resolved spin polarization  $P$  is independent of the carrier populations at that energy. A reduced carrier concentration in the investigated energy interval will only lead to an increased statistical error on the measured spin polarization.

In order to study the spin decay in the band bent region by TR-2PPE, we first excite spin-polarized electrons with a circularly polarized fs-laser pulse at

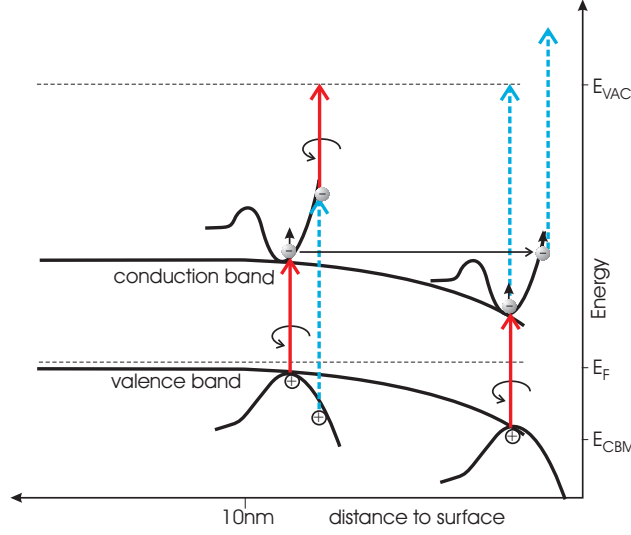


**Fig. 6.** Bichromatic 2PPE-process in a surface region with band bending. By making use of the energy resolution of the photoemission technique, we can probe the hot electron spin dynamics at different energy levels. Parts of the band structure at different distances from the surface are sketched. The solid arrows mark the transitions induced by the absorption of 1.55 eV pump photons, and the dashed arrows the transitions induced by the 3.1 eV probe photons.

$\hbar\omega = 1.55$  eV, slightly larger than the bandgap. Some of the spin-polarized hot electrons will move towards the band-bending area, where the carriers become hot (see Fig. 6) and will undergo different elastic and inelastic relaxation processes. The spin dependent depletion of the excited-state population in the surface region can be determined by a suitably delayed second laser pulse which photoemits the electrons. The second (probe) laser pulse must be at higher photon energy ( $\hbar\omega = 3.1$  eV) in order to overcome the vacuum energy.

## 4.2 Experimental Setup

The laser system used is by now a standard tool for measurements of the type described here. It consists of a mode locked Titanium-doped Sapphire (Ti:Al<sub>2</sub>O<sub>3</sub>) laser, pumped by a diode laser at about 8 W. This setup generates transform-limited and sech<sup>2</sup> temporally shaped pulses of up to 15 nJ/pulse with a duration of less than 45 fs at a repetition rate of 82 MHz. The wavelengths of the pulses can be tuned from 830 to 770 nm, thereby varying the photon-energy from 1.49 eV to 1.61 eV. For the time resolved experiments the pulse train is split by a beam splitter (see Fig. 7). By varying the optical path with a variable delay line, we can shift the two pulse trains by a certain length corresponding to a delay in time.

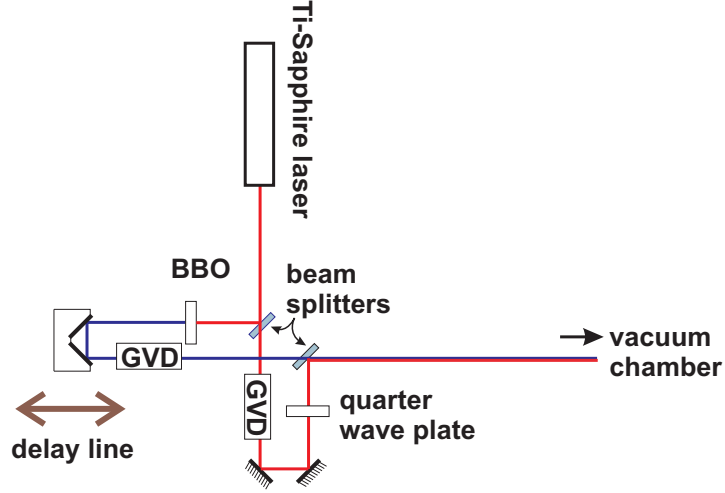


**Fig. 7.** Schematic set-up of the Mach-Zehnder-interferometer. The pulses are split up and can be delayed with respect to each other. In addition, we can modify each arm of the interferometer to tailor the beam properties to our specific needs by introducing e.g. frequency doubling elements or quarter wave plates. Each arm then needs individual dispersion compensation.

The pulse of one path is frequency doubled by a thin  $\beta$ -barium-borate-(BBO-)crystal to yield photon energies in the range of 3.0 to 3.2 eV (in the following designated by *blue*). The pulse of the other path (fundamental, in the following designated by *red*), is transformed from linearly polarized to circularly polarized by introducing a quarter-wave plate. Adjusting the quarter wave plate, we can change between left-handed and right-handed light. This setup is used for the optical orientation experiments. The frequency-doubled pulses remain linear. After delaying, the pulses are re-united by a second beam splitter and then focused by a lens onto the sample inside the UHV-chamber. The polarized laser beam is incident perpendicular on the sample surface, and the electrons are detected at an angle of  $45^\circ$  with respect to the surface normal. In order to account for the pulse broadening introduced into the system by dispersive elements, a group velocity dispersion compensation is necessary for both pulse trains. This is accomplished with a prism pair traversed twice by the laser pulse resulting in negative dispersion, which cancels out the usually positive dispersion due to lenses and the vacuum viewport.

The laser-beams are adjusted to reach excitation densities as low as  $1 \times 10^{16} \text{ cm}^{-3}$ . The excitation densities are of the same order of magnitude for the fundamental laser beam and for the frequency doubled pulses, although the intensities are approximately 100 times smaller for the 3.1 eV pulses. This is due to the fact that the penetration depth for 3.1 eV photons is 50 times smaller than for the 1.55 eV photons. Considering the laser intensities used

and the absorption lengths  $\lambda$  at a wavelength of 800 nm ( $\lambda_r = 730$  nm) and 400 nm ( $\lambda_b = 14$  nm) in GaAs, we can roughly estimate the average excitation density from the laser power. Assuming a Gaussian profile for our laser beam, we determine the focus spot size of our lens to 100  $\mu\text{m}$  in diameter. Taking the maximum laser powers available, we can reach excitation densities on the order of  $5 \times 10^{18}$  electron-hole pairs  $\text{cm}^{-3}$ . By reducing the pulse-power (reducing the laser output and/or lowering the frequency doubling efficiency), more than three orders of magnitude in excitation density are available.

The time-averaged photocurrent at a fixed kinetic energy is measured as a function of the delay between the two beams (two pulse correlation technique). The nonlinearity of the two-photo process leads to an increase in the 2PPE yield when the pulses are spatially and temporarily superimposed. As long as the two laser pulses overlap in time, it is obvious that an electron can be emitted by absorbing just one photon from each pulse. However, if the pulses are separated in time an excited electron from the first pulse can absorb a photon from the second pulse only as long as the inelastic lifetime of the intermediate state exceeds the delay.

The samples are mounted in a UHV chamber (base pressure  $5 \times 10^{-11}$  mbar) equipped with a cylindrical sector electron energy analyzer. To investigate the electron dynamics separately for both spin directions, a spin analyzer (SPLEED-detector [40, 41]) is mounted on top of the electron-energy analyzer. This makes the measurement of one in-plane component of the spin-polarization vector possible. A bias voltage of  $-14$  V is applied to the sample to eliminate the effects of any stray electric and magnetic fields.

As sample we use a p-doped (100) oriented GaAs crystal with dopant concentration (zinc)  $N_A = 1 \times 10^{19} \text{cm}^{-3}$ . GaAs surfaces are quite reactive when exposed to air and the surface of a sample stored outside a vacuum chamber is oxidized. The samples are cleaned by etching in sulfuric acid and rinsing, followed by heating to approximately  $500^\circ\text{C}$  in the UHV chamber. Prior to the measurements the sample is treated with a small amount of cesium in order to obtain a well-defined Fermi-level pinning and a lowered work function [38].

### 4.3 Experimental Results for GaAs (100)

By making use of the energy resolution of the photoemission technique one can probe the spin polarization of the hot electrons at different energy levels in the band-bending region. Figure 8 shows the spin polarization versus energy at zero delay time when there is temporal overlap of the pump and probe pulses. The reference energy is the conduction band minimum (CBM) at the surface ( $E_{\text{CBM}}$ ). We observe nearly uniform spin polarization within the band-bending energy range. Taking into account that the electrons close to the conduction band minimum have undergone many elastic and inelastic scattering processes, the result indicates that the spin relaxation in the



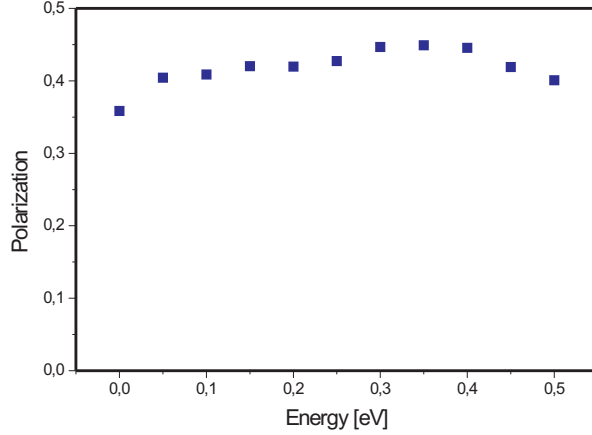


**Fig. 8.** Spin polarization of photoexcited electrons ( $\hbar\omega = 1.55$  eV), injected into the (100) surface of a GaAs-crystal with band bending. The zero of the energy scale is defined as the conduction band minimum at the surface ( $E_{CBM}$ ) and represents the energy of the intermediate state after absorption of the first photon.

band-bending region must occur on a much longer time scale than the energy relaxation-time. This has been questioned previously by several authors considering hot electrons [42, 26, 39].

In the following time dependent measurements we keep the energy of the detected photoelectrons constant and vary the temporal delay between the exciting pulse (which yields the spin polarization) and the probing pulse. As discussed in Sec. 4.2, we use the bichromatic 2PPE method, where pump (*red*) and probe (*blue*) laser have different photon energies.

In a bichromatic experiment electrons can be excited in two different ways (see Fig. 9). With photons of 1.55 eV average energy and circular polarization (*red*) we create a spin aligned population with a spin-polarization of 50% in theory or approximately 40% at room temperature. These electrons are excited with a small excess energy near the  $\Gamma$  point (see Figs. 9a and 9b). The second kind of electrons are excited by linearly polarized photons of 3.1 eV (*blue*) leading to a non-polarized and highly excited population in the conduction band (see Figs. 9c and 9d). In a second step this population may gain additional energy by other photons. Let us consider electrons absorbing enough energy to reach the vacuum level, which can be properly adjusted by a treatment of the surface with alkali atoms such as Cs. It is obvious that the bichromatic transitions (*red-blue* and *blue-red* transitions) are delay dependent since they involve photons of both pulses. The monochromatic contributions (*blue-blue* or *triple red*) are delay independent since they occur independently of the other laser pulse. Hence, monochromatic transitions will dominate the signal at long delay times ( $\Delta t \rightarrow \pm\infty$ ), when the pulses are

well separated, whereas the bichromatic events will dominate at delay times within the energetic relaxation time of the electron.

The first event in these multiphoton processes is a direct interband transition and, therefore, not only the intermediate, but also the initial and final state will be energetically distinguishable between the two processes (see Fig. 9). This results in a different kinetic energy of the *blue-red* and the *red-blue* transition photoelectrons and they can be separated by means of an energy analyser. In the band bending region, however, we cannot energetically discriminate between the *red* excited populations and the *blue* excited electrons completely. The energy of the initial state (relative to the vacuum energy) varies as a function of the distance to the surface, resulting in partly overlapping energy ranges of *red-blue* and *blue-red* events, see Fig. 6. Next to the intermediate state close to the conduction band minimum (probed due to a *red-blue* process) one also probes a higher lying state due to the *blue-red* process. Therefore, working in the bichromatic mode one has to consider, that the signal is given by the dynamics of both probed intermediate state. In a semiconductor, however, the dynamics of both probed intermediate states do not interfere with each other. Figure 10(a) shows the 2PPE photocurrent as a function of the pump-probe delay time. Positive (negative) delay time corresponds to *red-blue* (*blue-red*) transitions. The dotted curve shows the cross correlation of the laser pulses (photon fluence) given by the 2PPE yield vs. delay time on a transition metal surface with very short relaxation times. The result shows that the part of the measured signal due to *blue-red* transitions,

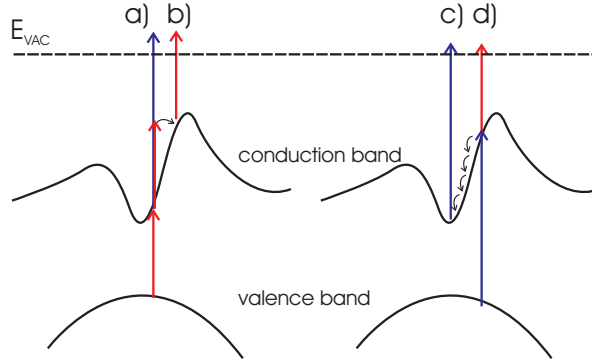


**Fig. 9.** Multiphoton processes: a) *red-blue* transition yielding spin polarization if the *red* pulse is circularly polarized. b) *triple red* transition yielding also spin polarization. c) *blue-blue* transition involving inelastic scattering events. d) *blue-red* transition. Both c) and d) yield zero spin polarization because the *blue* pulse is linearly polarized. These events occur in overlapping energetic regions, when the experiment is carried out in the band-bending surface area.

which transit via the higher excited intermediate states (see Fig. 9), shows a much faster population decay compared to the *red-blue* part, which probes the dynamics close to the conduction band minimum. Hence, due to the large difference in the population decay between *red-blue* and *blue-red* transition, we can distinguish very easily between these two (in general interfering) 2PPE processes. The simultaneously measured spin-polarization of the photoelectrons is illustrated in Fig. 10(b). We can divide our polarization data curves into three different regimes:

- Regime I: Excitation with linearly polarized 3.1 eV and emission with circular 1.55 eV-photons at a negative delay of 250 fs or more. The comparatively weak signal is dominated by background electrons such as spin-polarized 3-photon-processes of 1.55 eV photons (see Fig. 9b) and unpolarized electrons of 2-photon-processes of 3.1 eV photons (see Fig. 9c) which lost energy in a scattering event. This regime is characterized by a low count rate and therefore high noise in spin signal.
- Regime II: overlapping regime: the pulses overlap in time and, hence, bichromatic transitions dominate. The left shift of the 2PPE cross-correlation curve compared to time zero indicates that unpolarized *blue-red* transitions dominate over polarized *red-blue* transitions, resulting in a strongly reduced spin polarization of the detected photoelectrons. In this region we find a strong signal and very accurate spin determination.
- Regime III: *red-blue* transition at a delay  $> 200$  fs. The region with the highest spin polarization, since the signal is dominated by optically induced spin polarized electrons close to the conduction band edge. These intermediate states are long-lived leading to a high count rate over a wide delay range. Observing the spin polarization with increasing delay time allows the determination of the spin relaxation-time  $T_1$  as long as the energetic relaxation is not much faster than the spin relaxation.

In the following we will discuss the spin decay processes at the conduction band minimum and 200 meV above. Figure 11 shows the spin polarization versus positive delay time (*red-blue* transitions) for hot electrons at 200 meV above the conduction band minimum. The excess energy is a multiple of the longitudinal optical phonon energy  $\hbar\omega_p = 36$  meV, but it is lower than the split-off valence-band energy  $\Delta_{SO} = 340$  meV. The data were corrected for the decaying electron population under the assumption that the background contributions from the two pulses (*blue-blue* and *triple red*) remain constant for all delays. Since the transient population of excited electrons decays quite fast on a time scale of a few 100 fs, the noise level increases considerably over delay time. The polarization shows no spin relaxation on our time scale of about 20 ps in length. The dash-dotted curve is a fit with  $T_1 = 60$  ps, which represents

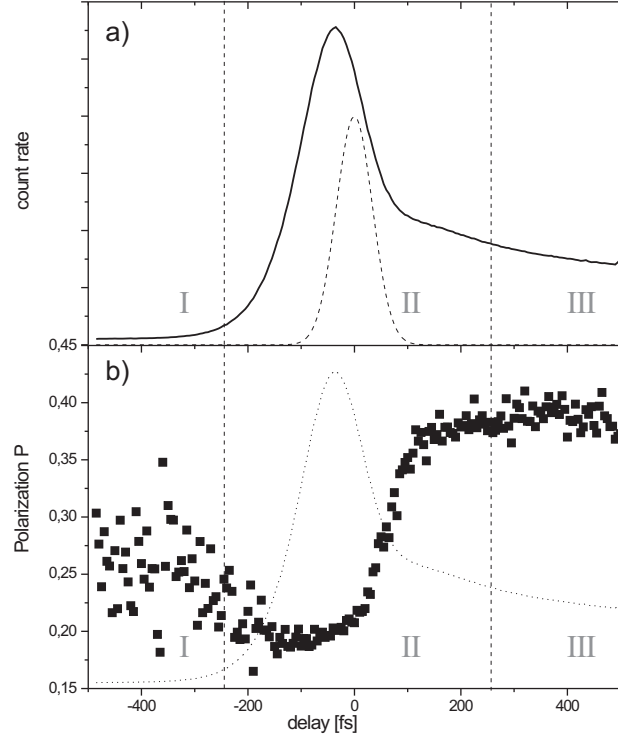


**Fig. 10.** (a) 2PPE photo-current as a function of the pump-probe delay time. The dotted curve shows the cross-correlation of the laser-pulses (photon-fluence). (b) Spin dynamics around short delays, the dotted curve is a replica from (a). We can distinguish 3 regimes. From left to right: I. *blue-red* regime: The low count rate is mainly given by background electrons from 3-photon-absorption (see Fig. 9). II. Overlapping regime: Spin drops drastically due to highly excited unpolarized electrons, which decay very fast. III. *Red-blue* regime: constant spin polarization on the ps-timescale.

the GaAs bulk value expected from our theoretical analysis and experimentally verified for the same sample by means of time-resolved Faraday rotation at  $T = 300$  K. The fact that the spin polarization remains constant over the investigated delay time indicates that all additional quasi-elastic scattering processes in the band-bending region, e.g., at steps, defects, and impurities do not cause spin flips. Compared to the bulk, the spin relaxation of hot electrons in the interface is slower.

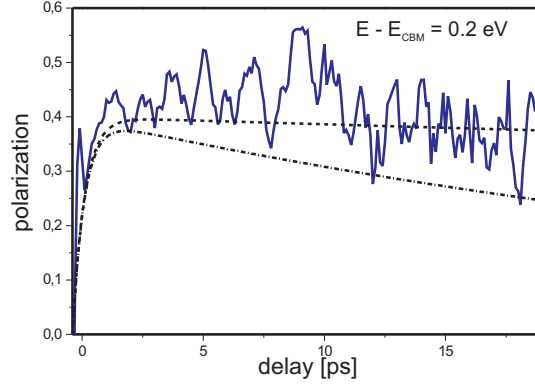


**Fig. 11.** Spin polarization vs. delay time for hot electrons at 0.2 eV above conduction band minimum at the surface. The dashed curve corresponds to a spin decay on the order of 300 ps. The dash-dotted curve represents a spin decay time of 60 ps.

In Fig. 12 the spin-polarization versus positive delay time is shown for electrons at the conduction band minimum of the surface. No direct excitation is possible using photon energies at 1.55 eV (bandgap energy at room temperature:  $E_g = 1.42$  eV). Time-resolved measurements show that the population increases at zero delay and reaches its maximum at a delay of 100 fs. Hence, the electrons in this energy interval have been generated either in the band-bending region at the surface or in the bulk and have diffused towards the surface. The carriers have undergone many inelastic scattering processes, none of them includes a spin-flip process as clearly shown in Fig. 12 for longer time delays.

Again, the spin relaxation rate in the interface is decreased compared to the bulk value (dotted line) as determined by the time-resolved Faraday rotation experiment. Our experimental data show a lower limit for  $T_1$  of more than 300 ps. It should be noted that for p-doped semiconductors a much faster population decay of the carriers compared to the spin decay makes the exact determination of  $T_1$  difficult by means of a real time experiment.

#### 4.4 Comparison between Experimental and Theoretical Results

For the p-doping concentration considered here, the BAP process, i.e., the electron-hole exchange interaction, is considered to be the dominating contribution to spin relaxation [17]. The reason for the experimental result is shown by our calculations: To obtain reliable spin relaxation-times one has to compute the time development of the distribution functions for spin-up and spin-down electrons including the relevant scattering mechanisms and accounting for in and out-scattering events, thus going beyond existing evaluations of the spin relaxation at the level of Fermi's Golden Rule [21, 17]. In the case

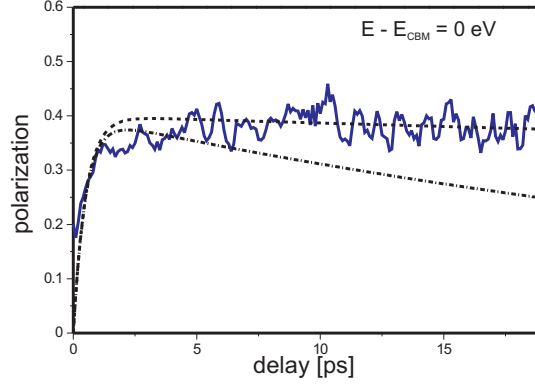


**Fig. 12.** Spin polarization versus delay-time at conduction band minimum. As a guide to the eye, the dashed curve corresponding to a spin decay on the order of 300 ps. The dash-dotted curve represents the bulk value of  $T_1 = 60$  ps, as obtained by a time-resolved Faraday rotation experiment.

of strongly p-doped GaAs these scattering mechanisms are electron-hole exchange scattering, which is comparatively slow but can flip the electron spins, and electron-hole direct Coulomb scattering, which is much faster and cannot flip spins. Because the exchange scattering alone does not lead to a thermalization between electrons and holes, the direct scattering process, which does lead to this thermalization, is needed to provide physically sensible results if the electronic distributions are tracked over several tens of picoseconds. From the time development of the electronic distribution functions one then calculates the spin relaxation and determines the relaxation time by an exponential fit. This procedure yields energy-dependent spin polarizations whose relaxation times have only a very weak energy dependence, in contrast to the rates leading to the spin relaxation.

Since the experimental results presented above were obtained using 2PPE, where the spin polarization is measured for electrons from the surface or interface region of the semiconductor, we can assess the spin relaxation in the semiconductor/metal interface region. The electrons that are detected in the interface region have been optically excited in the bulk of the semiconductor by the *red* laser pulse and have then reached the interface region with strong band bending. It has been argued that the electrons are subject to efficient scattering process when they reach the band bending region where they become “hot” and thus that their spin-polarization should relax more quickly than in the bulk.[39] Our experimental results show the opposite effect: The spin relaxation-time is significantly longer than the corresponding value for electrons in the bulk. The explanation for this behavior is that the electrons in the interface region are effectively separated from a high hole density because they become effectively localized in the potential well formed by the down-

ward slope of the electron band and the surface. In the surface region, on the other hand, the concentration of holes is strongly reduced because of the depletion of holes close to the interface in a Schottky barrier. This explanation is supported by our calculations: We see from Fig. 4 that the relaxation time is indeed very sensitive to the hole concentration, and that the relaxation time thus is a measure of the hole concentration in the interface region. Using the experimental value of 300 ps relaxation time, we obtain the rough estimate of a 40% decrease in hole concentration at the surface from Fig. 4.

For the comparison between theory and experiment presented above, we have taken the theoretical bulk spin relaxation-time as a measure of the spin relaxation at the interface and we have allowed the hole concentration to vary over several orders of magnitude. For lower doping concentrations, it is expected that a contribution from the DP process will also come into play and some details of the scattering mechanisms can also be affected by the localization of the electrons close to the surface, which essentially restricts them to move in a two-dimensional layer. There is as yet no straightforward explanation for the reduced DP process at the interface. One may assume a preferential orientation of the conduction electron momentum in the (100) direction of the GaAs interface caused by the electric field in the band bending region. Taking into account that there is no spin splitting of the conduction band along the (100) axis of GaAs [26], this alignment effect can reduce the spin relaxation due to the precession along the internal field. A quantitative theoretical analysis of the influence of the DP process, as well as an inclusion of the reduced dimensionality of the electron gas at the interface are left for future investigations

We thank B. Beschoten for helpful discussions and sharing his experimental results before publication. We are grateful to M. Bauer, M. Fleischhauer, W. Hübner, and S. W. Koch for helpful discussions. Financial support from the DFG and a CPU grant from the Forschungszentrum Jülich are gratefully acknowledged.

## References

1. G. A. Prinz. Device physics—magnetoelectronics. *Science*, 282:1660, 1998.
2. L. J. Sham. Semiconductor devices—closer to coherence control. *Science*, 277:1258, 1997.
3. H. Akinaga and H. Ohno. Semiconductor spintronics. *IEEE Transactions on Nanotechnology*, 1:19, 2002.
4. J. M. Kikkawa and D. D. Awschalom. Resonant spin amplification in n-type GaAs. *Phys. Rev. Lett.*, 80:4313, 1998.
5. G. Schmidt, D. Ferrand, L. W. Molenkamp, A. T. Filip, and B. J. van Wees. Fundamental obstacle for electrical spin injection from a ferromagnetic metal into a diffusive semiconductor. *Phys. Rev. B*, 62:R4790, 2000.
6. B. T. Jonker. Progress toward electrical injection of spin-polarized electrons into semiconductors. *Proceedings of the IEEE*, 91:727, 2003.

7. D. D. Awschalom, D. Loss, and N. Samarth, editors. *Semiconductor Spintronics and Quantum Computation*. Springer, Berlin, 2002.
8. E. Johnston-Halperin, D. Lofgreen, R. K. Kawakami, D. K. Young, L. Col-dren, A. C. Gossard, and D. D. Awschalom. Spin-polarized Zener tunneling in (Ga,Mn)As. *Phys. Rev. B*, 65:041306, 2002.
9. S. A. Crooker, D. D. Awschalom, J. J. Baumberg, F. Flack, and N. Samarth. Optical spin resonance and transverse spin relaxation in magnetic semiconductor quantum wells. *Phys. Rev. B*, 56:7574, 1997.
10. S. Hallstein, J. D. Berger, M. Hilpert, H. C. Schneider, W. W. Rühle, F. Jahnke, S. W. Koch, H. M. Gibbs, G. Khitrova, and M. Oestreich. Manifestation of coherent spin precession in stimulated semiconductor emission dynamics. *Phys. Rev. B*, 56:R7076, 1997.
11. P. Y. Yu and M. Cardona. *Fundamentals of Semiconductors*. Springer, Berlin, 3. edition, 2001.
12. G. L. Bir and G. E. Pikus. *Symmetry and Strain-Induced Effects in Semiconductors*. Wiley, New York, 1974.
13. E. L. Ivchenko and G. E. Pikus. *Superlattices and Other Heterostructures*. Springer, Berlin, 2. edition, 1997.
14. R. Winkler. *Spin-Orbit Coupling Effects in Two-Dimensional Electron and Hole Systems*. Springer, Berlin, 2003.
15. G. E. Pikus and A. N. Titkov. Spin relaxation under optical orientation in semiconductors. In F. Meier and B. P. Zakharchenya, editors, *Optical Orientation*, pages 73–131. North-Holland, Amsterdam, 1984.
16. C. Kittel. *Quantum Theory of Solids*. Wiley, 1987.
17. P. H. Song and K. W. Kim. Spin relaxation of conduction electrons in bulk III-V semiconductors. *Phys. Rev. B*, 66:035207, 2002.
18. M. I. Dyakonov and V. I. Perel. Spin orientation of electrons associated with interband absorption of light in semiconductors. *Soviet Physics JETP*, 33:1053, 1971.
19. G. L. Bir, A. G. Aronov, and G. E. Pikus. Spin relaxation of electrons due to scattering by holes. *Sov. Physics JETP*, 42:705, 1976.
20. G. E. Pikus and G. L. Bir. Exchange interaction in excitons in semiconductors. *Sov. Physics JETP*, 33:208, 1971.
21. M. Z. Maialle. Spin relaxation of electrons in p-doped quantum wells via the electron-hole exchange interaction. *Phys. Rev. B*, 54:1967, 1996.
22. L. Reichl. *A Modern Course in Statistical Physics*. University of Texas Press, Austin, 1980.
23. B. A. Sanborn, B. Y. K. Hu, and S. Das Sarma. Correction to the decay rate of nonequilibrium carrier distributions due to scattering-in processes. *Phys. Rev. B*, 49:7767, 1994.
24. I. Žutić, J. Fabian, and S. Das Sarma. Spintronics: Fundamentals and applications. *Rev. Mod. Phys.*, 76:323, 2004.
25. L. J. Sham. Theory of spin coherence in semiconductor heterostructures. *J. Magn. Magn. Mater.*, 200(1-3):219, 1999.
26. F. Meier and B. P. Zakharchenya, editors. *Optical Orientation*. North-Holland, Amsterdam, 1984.
27. M. M. Glazov and E. L. Ivchenko. Precession spin relaxation mechanism caused by frequent electron-electron collisions. *JETP Letters*, 75:403, 2002.
28. M. Q. Weng and M. W. Wu. Spin-dephasing in n-type GaAs quantum wells. *Phys. Rev. B*, 68:075312, 2003.



29. M. W. Wu and H. Metiu. Kinetics of spin coherence of electrons in an undoped semiconductor quantum well. *Phys. Rev. B*, 61:2945, 2000.
30. C. Lechner and U. Rössler. An extension of the optical bloch equations: a microscopic approach including spin and carrier-phonon scattering, 2004. cond-mat/0412370.
31. W. Schäfer and M. Wegener. *Semiconductor Optics and Transport Phenomena*. Springer, 2002.
32. R. Binder and S. W. Koch. Nonequilibrium semiconductor dynamics. *Progress Quant. Electronics*, 19:307, 1995.
33. M. Kira, F. Jahnke, W. Hoyer, and S. W. Koch. Quantum theory of spontaneous emission and coherent effects in semiconductor microstructures. *Progress Quant. Electronics*, 23:189, 1999.
34. F. Rossi and T. Kuhn. Theory of ultrafast phenomena in photoexcited semiconductors. *Rev. Mod. Phys.*, 74:895, 2002.
35. H. Haug and S. W. Koch. *Quantum Theory of the Optical and Electronic Properties of Semiconductors*. World Scientific, Singapore, 4. edition, 2004.
36. B. Beschoten, E. Johnston-Halperin, D. K. Young, M. Poggio, J. E. Grimaldi, S. Keller, S. P. DenBaars, U. K. Mishra, E. L. Hu, and D. D. Awschalom. Spin coherence and dephasing in GaN. *Phys. Rev. B*, 63:121202, 2001.
37. A. Sutton and R. Balluffi. *Interfaces in Crystalline Materials*. Oxford UP, Oxford, 1995.
38. W. Mönch. *Semiconductor Surfaces and Interfaces*. Springer Series in Surface Sciences. Springer, Berlin, 3. edition, 2001.
39. D. T. Pierce and F. Meier. Photoemission of spin-polarized electrons from GaAs. *Phys. Rev. B*, 13:5484, 1976.
40. M. Aeschlimann, M. Bauer, S. Pawlik, W. Weber, R. Burgermeister, D. Oberli, and H. C. Siegmann. Ultrafast spin-dependent electron dynamics in fcc Co. *Phys. Rev. Lett.*, 79:5158, 1997.
41. J. Kirschner. Sources and detectors for polarized electrons. In R. Feder, editor, *Polarized Electrons in Surface Physics*. World Scientific, Singapore, 1985.
42. F. Bentivegna, P. Yvernault, A. V. Petukhov, and T. Rasing. Time-resolved photo-induced nonlinear magneto-optical Kerr effect for the study of spin dynamics at a GaAs (001) surface. *Applied Physics B*, 68:519, 1999.